University of Groningen

Cadmium isotope variations in the Southern Ocean

Xue, Zichen; Rehkämper, Mark; Horner, Tristan J.; Abouchami, Wafa; Middag, Rob; Flierd, Tina van de; de Baar, Hein J.W.

IMPORTANT NOTE: You are advised to consult the publisher's version (publisher's PDF) if you wish to cite from it. Please check the document version below.

Document Version
Publisher's PDF, also known as Version of record

Link to publication in University of Groningen/UMCG research database

Cadmium isotope variations in the Southern Ocean

Zichen Xue [a], Mark Rehkämper [a,*], Tristan J. Horner [b,c], Wafa Abouchami [d,e],
Rob Middag [f,g], Tina van de Flierd [a], Hein J.W. de Baar [f]

[a] *Department of Earth Science and Engineering, Imperial College London, London SW7 2AZ, UK*
[b] *Department of Earth Sciences, University of Oxford, Oxford OX1 3AN, UK*
[c] *Department of Marine Chemistry and Geochemistry, Woods Hole Oceanographic Institution, Woods Hole, MA 02543, USA*
[d] *Institut für Mineralogie, WWU Münster, 48149 Münster, Germany*
[e] *Max Planck Institute for Chemistry, P.O. Box 3060, 55020 Mainz, Germany*
[f] *Royal Netherlands Institute for Sea Research, P.O. Box 59, 1790 AB Den Burg, The Netherlands*
[g] *Department of Chemistry, University of Otago, P.O. Box 56, Dunedin 9054, New Zealand*

A B S T R A C T

Cadmium concentrations and isotope compositions were determined for 47 seawater samples from the high nutrient low chlorophyll (HNLC) zone of the Atlantic sector of the Southern Ocean. The samples include 13 surface waters from a transect of the Weddell Gyre and 3 depth profiles from the Weddell Sea and Drake Passage. The Southern Ocean mixed layer samples from this study and Abouchami et al. (2011) define a clear but broad 'HNLC trend' in a plot of $\varepsilon^{114/110}$Cd versus [Cd], which is primarily a consequence of isotopic fractionation associated with biological uptake ($\varepsilon^{114/110}$Cd is the deviation of the ^{114}Cd/^{110}Cd ratio of a sample from NIST SRM 3108 Cd in parts per 10,000). The trend is especially apparent in comparison to the large range of values shown by a global set of seawater Cd data for shallow depths. The Southern Ocean samples are also distinguished by their relatively high Cd concentrations (typically 0.2 to 0.6 nmol/kg) and moderately fractionated $\varepsilon^{114/110}$Cd (generally between +4 and +8) that reflect the limited biological productivity of this region. Detailed assessment reveals fine structure within the 'HNLC trend', which may record differences in the biological fractionation factor, different scenarios of closed and open system isotope fractionation, and/or distinct source water compositions.
Southern Ocean seawater from depths ⩾1000 m has an average $\varepsilon^{114/110}$Cd of +2.5 ± 0.2 (2se, $n = 16$), and together with previous results this establishes a relatively constant $\varepsilon^{114/110}$Cd value of +3.0 ± 0.3 (2se, $n = 27$) for global deep waters. Significant isotopic variability was observed at intermediate depths in the Southern Ocean. Seawater from 200 m to 400 m in Weddell Sea has high Cd concentrations and $\varepsilon^{114/110}$Cd as low as +1, presumably due to remineralization of Cd from biomass that records incomplete nutrient utilization. Antarctic Intermediate Water, which was sampled at 150 to 750 m depth in the Drake Passage, features a distinct Cd isotope signature of $\varepsilon^{114/110}$Cd $\approx$ +4, which reflects biological isotope fractionation at the surface and subsequent mixing into the ocean interior. Taken together, our results demonstrate that coupled Cd isotope and concentration data provide valuable insights into the distribution and biological cycling of Cd in the water column. The highly systematic nature of Cd isotope signatures may furthermore prove to be of utility for future research in marine geochemistry and paleoceanography.

© 2013 Elsevier B.V. All rights reserved.

1. Introduction

Cadmium is a trace element with a marine distribution similar to that of dissolved phosphate, thereby suggesting that seawater Cd concentrations are also controlled by phytoplankton uptake in surface waters and remineralization of organic matter at depth (Boyle et al., 1976; Bruland, 1980; Nolting and de Baar, 1994). A biochemical function for Cd has, furthermore, been demon-strated in some marine diatoms (Price and Morel, 1990), where Cd can replace Zn in the metalloenzyme carbonic anhydrase (Lane et al., 2005; Xu et al., 2008). The extent to which this substitution can account for the marine distribution of Cd has, however, recently been challenged (Horner et al., 2013).

Considerable Cd isotope fractionations were revealed in recent seawater studies and applied to investigate the marine cycling of this transition metal. Nutrient and Cd depleted surface waters can exhibit $\varepsilon^{114/110}$Cd values as high as +20 to +40, as a result of isotope fractionation during biological utilization ($\varepsilon^{114/110}$Cd represents the deviation of ^{114}Cd/^{110}Cd for a sample relative to the
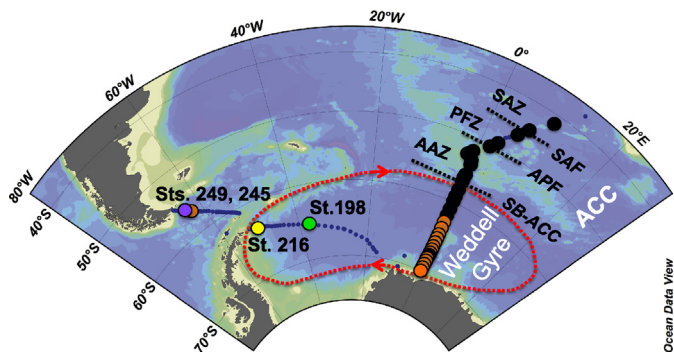
Fig. 1. Location map for Southern Ocean seawater samples analyzed and discussed in this study. New data are presented for three depth profiles at Stations 198 (Weddell Sea), 216 (Antarctic Peninsula), and 249 (Drake Passage), as well as 13 surface waters from the Zero Meridian between 62° and 69°S and an upper mixed layer sample from Station 245 in the Drake Passage (orange symbols). Black dots are surface waters from the study of Abouchami et al. (2011), whilst small blue dots show other sampling stations of the cruise (which thereby define the cruise track). The location of the Weddell Gyre is denoted by the red dashed line. Other abbreviations demark important hydrographic regions: ACC = Antarctic Circumpolar Current, SAZ = Subantarctic Zone, PFZ = Polar Frontal Zone, AAZ = Antarctic Zone, SAF = Subantarctic Front, APF = Antarctic Polar Front, SB-ACC = Southern Boundary of the ACC.

NIST 3108 Cd reference material in parts per 10,000). In contrast, the deep ocean appears to be characterized by relatively constant $\varepsilon^{114/110}$Cd values of about +2.5 to +3.0 (e.g., Lacan et al., 2006; Ripperger et al., 2007; Gault-Ringold et al., 2012; Xue et al., 2012)

The study of Abouchami et al. (2011) was the first to investigate the Cd isotope composition of Southern Ocean surface seawater and this region is of particular interest, because the Southern Ocean constitutes by far the largest of the three major HNLC (high nutrient low chlorophyll) regions of the world ocean. The HNLC regions are characterized by relatively low amounts of biomass even though the major nutrients nitrate, phosphate and silicate are sufficiently abundant to support phytoplankton growth (Nelson and Smith, 1991). Previous studies have suggested that nutrient utilization in the Southern Ocean HNLC area is limited by the availability of Fe, a key marine trace nutrient, and light (de Baar et al., 1990, 1995; Martin et al., 1990; Sunda and Huntsman, 1997).

The present investigation follows up on the study of Abouchami et al. (2011) with coupled Cd isotope and concentration analyses for almost 50 seawater samples that were collected during the same sampling campaign. Our results for both a surface transect and three depth profiles thus significantly enlarge the limited Cd isotope dataset currently available for the Southern Ocean. Combining both datasets, we systematically investigate the processes that govern the distribution and cycling of Cd in this HNLC region.

2. Samples and sampling region

Cadmium concentrations and isotope compositions were determined for 47 seawater samples that were collected between February and March 2008 during the GEOTRACES expedition ANT XXIV/3 aboard the RV Polarstern. This includes 34 samples from three vertical profiles in the Weddell Sea (Station 198), near the Antarctic Peninsula (Station 216) and the northern Drake Passage (Station 249) and 13 surface water samples from the Zero Meridian between 62° and 69°S in the Weddell Gyre (Fig. 1, Table 1; Supplement Section 1). The latter samples continue and complete the Cd isotope surface water transect that was recently published by Abouchami et al. (2011) on samples from the same cruise (Supplement Section 1).

The vertical profile samples were collected with an ultraclean CTD system (de Baar et al., 2008), whilst the surface waters were obtained at 2–5 m depth with an ultraclean IFISH torpedo and

pumpline system. After collection, the samples were immediately filtered using 0.2 µm nominal size cutoff filter cartridges into precleaned bottles and acidified to about pH 2 using distilled 6 M HCl. Further details of the sampling techniques are available in Middag et al. (2011).

Together, the water samples analyzed here and by Abouchami et al. (2011) comprehensively characterize the HNLC conditions of the Southern Ocean, encompassing (from north to south; Fig. 1): (i) the Subantarctic Zone (SAZ) north of the Subantarctic Front (SAF) at ∼45°S; (ii) the Antarctic Circumpolar Current (ACC) comprising the Polar Frontal Zone (PFZ; ∼45°S to 51°S) that extends from the SAF to the Antarctic Polar Front (APF) and the Antarctic Zone (AAZ; ∼51–56°S) from the APF to the Southern Boundary of the ACC (SB-ACC); and (iii) the Weddell Gyre south of ∼56°S.

Numerous water masses are encountered in this region but only aspects significant for the present study are mentioned below. The upwelling of Circumpolar Deep Water (CDW) in the Weddell Gyre and AAZ generates Antarctic Surface Water (AASW), which spreads northward, subducting north of the APF to contribute to the formation of Antarctic Intermediate Water (AAIW). Subantarctic Mode Water (SAMW), formed from deep winter mixed layers, overlies AAIW north of the SAF and export of both water masses occurs in northward direction. More detailed summaries of the circulation system and water masses present in the Atlantic sector of the Southern Ocean are provided elsewhere (e.g., Whitworth and Nowlin, 1987; Orsi et al., 1993, 1995; relevant studies from the ANT XXIV/3 expedition are listed in Supplement Section 2).

3. Analytical methods

The instruments and techniques that were employed for the acquisition of data for salinity and potential temperature, as well as oxygen and nutrient concentrations, are described elsewhere (Middag et al., 2011, 2012). The coupled Cd isotope composition and concentration analyses were carried out at the Imperial College MAGIC Laboratories, using recently published methods (Ripperger and Rehkämper, 2007; Xue et al., 2012). In brief, about 0.3 to 1.1 L of seawater were weighed to obtain at least 30 ng of natural Cd and a suitable volume of a ^{111}Cd–^{113}Cd double spike was added to achieve a spike to sample ratio of ∼1. A three-stage column chemistry was then employed for the separation of Cd at yields of better than 90% and with a total procedural Cd blank of ∼20 pg, equivalent to less than 0.1% of the indigenous Cd present in the samples. The isotopic analyses were carried out using a Nu Plasma HR MC-ICP-MS (multiple collector inductively coupled plasma mass spectrometer), with data being processed offline to calculate the Cd isotope compositions of the samples. In the following, these results are expressed as $\varepsilon^{114/110}$Cd values, which are given relative to the NIST SRM 3108 Cd isotope standard (std):

$$\varepsilon^{114/110}\text{Cd} = \left(\left[\left(^{114}\text{Cd}/^{110}\text{Cd}\right)_{\text{sample}}/\left(^{114}\text{Cd}/^{110}\text{Cd}\right)_{\text{std}}\right] - 1\right)$$
$$\times 10{,}000$$

Additional analyses of the secondary Cd isotope reference materials BAM-I012 Cd ($\varepsilon^{114/110}$Cd = −13.57 ± 0.60, 2sd; $n = 17$), JMC Cd Münster (−0.96 ± 0.21; $n = 25$), and Alfa Cd Zurich (−0.61 ± 0.29; $n = 17$) were carried out during measurement sessions, to monitor data quality and all results showed excellent agreement with consensus values (−13.32 ± 0.43, −0.89 ± 0.42, and −0.20 ± 0.51, respectively; Abouchami et al., 2012). Cadmium isotope data from the literature that were acquired relative to other zero-epsilon reference materials are reported here relative to NIST SRM 3108 Cd, based either on the community-consensus isotopic offsets between the standards (Abouchami et al., 2012) or the conversions given in the original publication.

Table 1

Cd concentrations and isotope compositions and other key data for the seawater samples analyzed in this study.

| Sampling Station	Latitude	Longitude	Depth (m)	Salinity	θ (°C)	[O$_2$] (µmol/kg)	[PO$_4^{3-}$] (µmol/kg)	[Si] (µmol/kg)	[NO$_3^-$] (µmol/kg)	[Cd] (nmol/kg)	$\varepsilon^{114/110}$Cd	±2sd
142	62.23°S	0.00	2–5	33.95	0.44		1.69	57.76	23.53	0.270	6.76	0.50
145	63.25°S	0.00	2–5	33.91	0.59		1.61	53.83	23.15	0.257	7.31	0.50
148	64.21°S	0.01°E	2–5	33.94	0.60		1.60	46.87	22.76	0.247	7.38	0.50
151	65.24°S	0.00	2–5	33.95	−0.24		1.62	62.49	25.14	0.378	5.39	0.50
153A	66.00°S	0.73°E	2–5	33.85	−0.21		1.61	61.97	25.52	0.373	6.34	0.50
156	66.52°S	0.01°E	2–5	33.8	−0.76		1.64	59.23	25.25	0.382	5.76	0.50
160	66.03°S	0.07°W	2–5	34.09	−0.41		1.63	58.70	25.41	0.263	7.48	0.68
162	66.56°S	0.00	2–5	33.84	−0.76		1.67	58.26	25.32	0.386	5.66	0.50
164	67.02°S	0.01°W	2–5	33.94	−0.73		1.77	65.49	26.77	0.434	4.75	0.70
166	67.58°S	0.00	2–5	33.93	−0.76		1.84	67.56	27.25	0.461	4.54	0.70
168	68.29°S	0.00	2–5	33.97	−0.74		1.78	62.87	26.40	0.413	4.83	0.71
170	68.65°S	0.00	2–5	33.93	−0.78		1.74	60.58	25.67	0.384	4.99	0.70
172	68.96°S	0.00	2–5	33.92	−1.02		1.75	60.50	25.66	0.390	5.00	0.50
198	65.61°S	36.40°W	25	34.16	−1.45	334.4	1.88	73.33	27.59	0.549	4.04	0.63
198	65.61°S	36.40°W	100	34.51	−1.73	292.0	2.11	83.56	30.59	0.719	2.59	0.35
198	65.61°S	36.40°W	200	34.67	0.24	196.2	2.36	112.35	34.17	0.890	1.68	0.39
198	65.61°S	36.40°W	300	34.67	0.23	196.2	2.38	120.64	34.43	0.888	1.35	0.35
198	65.61°S	36.40°W	400	34.68	0.38	191.0	2.39	118.49	34.41	0.882	0.98	0.35
198	65.61°S	36.40°W	500	34.69	0.40	191.4	2.39	121.52	34.39	0.863	2.48	0.23
198	65.61°S	36.40°W	1000	34.68	0.14	207.6	2.36	126.11	33.94	0.815	2.56	0.26
198	65.61°S	36.40°W	2000	34.66	−0.26	225.6	2.31	125.91	33.19	0.788	2.30	0.35
198	65.61°S	36.40°W	3000	34.66	−0.48	236.2	2.28	124.55	32.69	0.776	2.94	0.65
198	65.61°S	36.40°W	4000	34.65	−0.65	243.1	2.28	124.94	32.67	0.762	2.55	0.65
198	65.61°S	36.40°W	4702	34.64	−0.86	250.4	2.27	115.96	32.52	0.754	1.69	0.65
216	63.70°S	50.84°W	25	34.14	−1.85	306.0	2.05	73.04	28.80	0.645	4.65	0.82
216	63.70°S	50.84°W	100	34.43	−1.81	278.1	2.14	76.25	30.71	0.714	3.29	0.81
216	63.70°S	50.84°W	150	34.44	−1.81	275.8	2.14	77.03	30.78	0.739	2.41	0.23
216	63.70°S	50.84°W	200	34.46	−1.48	271.9	2.17	79.17	31.01	0.773	2.01	0.49
216	63.70°S	50.84°W	400	34.65	0.42	211.9	2.26	99.37	32.36	0.795	2.49	0.23
216	63.70°S	50.84°W	500	34.67	0.47	208.5	2.26	104.25	32.37	0.789	1.97	0.35
216	63.70°S	50.84°W	1000	34.68	0.33	211.3	2.29	115.96	32.87	0.783	2.23	0.49
216	63.70°S	50.84°W	1500	34.67	0.03	219.2	2.30	121.81	33.02	0.782	2.49	0.76
216	63.70°S	50.84°W	2000	34.66	−0.29	231.8	2.27	118.89	32.53	0.771	1.93	0.76
216	63.70°S	50.84°W	2450	34.61	−1.26	279.9	2.18	84.43	31.31	0.737	2.99	0.33
249	56.12°S	63.76°W	8.5	33.87	4.56	304.6	1.66	5.23	23.87	0.400	6.68	0.63
249	56.12°S	63.76°W	25	33.87	4.56	305.1	1.67	5.24	24.08	0.395	7.02	0.63
249	56.12°S	63.76°W	75	33.88	4.46	310.2	1.70	5.87	24.11	0.409	6.72	0.63
249	56.12°S	63.76°W	150	33.99	2.89	302.2	1.87	15.21	26.99	0.649	3.42	0.63
249	56.12°S	63.76°W	250	34.03	2.32	300.8	1.96	20.57	28.25	0.641	4.01	0.63
249	56.12°S	63.76°W	400	34.16	2.50	254.7	2.11	31.22	30.47	0.703	3.27	0.63
249	56.12°S	63.76°W	750	34.43	2.52	180.4				0.624	4.04	0.63
249	56.12°S	63.76°W	1250	34.64	2.18	163.9	2.30	79.43	33.16	0.807	2.46	0.35
249	56.12°S	63.76°W	1750	34.71	1.79	170.4	2.24	93.43	32.25	0.761	2.81	0.58
249	56.12°S	63.76°W	2500	34.73	1.30	186.9	2.21	104.12	31.89	0.744	2.40	0.58
249	56.12°S	63.76°W	3000	34.72	0.89	195.4	2.22	115.20	32.12	0.759	2.71	0.58
249	56.12°S	63.76°W	4000	34.69	0.36	210.9	2.24	120.37	32.44	0.763	2.50	0.58
249	56.12°S	63.76°W	4253	34.69	0.35	211.6	2.25	116.98	32.41	0.767	2.83	0.58
245	56.88°S	62.52°W	2–5	–	–	–	–	–	–	0.374	6.81	0.82

θ = potential temperature. The $\varepsilon^{114/110}$Cd values are reported relative to NIST SRM 3108 Cd (Abouchami et al., 2012). The quoted uncertainties for $\varepsilon^{114/110}$Cd are based on the ±2sd uncertainties determined for multiple analyses of matching standard solutions that were analyzed before and after each sample measurement. The Cd concentrations have an estimated uncertainty of about 1–2% (Xue et al., 2012). No hydrographic data (salinity, θ, [O$_2$]) are available for the sample from Station 245.

4. Results

4.1. Hydrography and nutrient concentrations for Zero Meridian surface seawater

In Fig. 2, the hydrographic and nutrient concentration data for the 13 Zero Meridian surface waters of this study (from 62.2°S to 69.0°S in the Weddell Gyre) are plotted together with the samples of Abouchami et al. (2011), which were collected primarily north of 61.2°S. Large gradients in nutrient content are clearly evident (Fig. 2), in agreement with previous observations (e.g., Sarmiento et al., 2004). North of the SAF, the SAZ features low [NO$_3^-$], [PO$_4^{3-}$] and [Si]. To the south, the ACC comprises the high [NO$_3^-$], [PO$_4^{3-}$] and low [Si] regime of the PFZ as well as the high [NO$_3^-$], [PO$_4^{3-}$], [Si] surface waters of the AAZ. The more southern Weddell Gyre is uniformly high in [NO$_3^-$], [PO$_4^{3-}$], [Si]. Hence only the AAZ and Weddell Gyre are truly HNLC for all three major nutrients.

Focusing on the Weddell Gyre data of the present study, the potential temperatures reveal two main groups of samples. Between 62.2°S and 64.2°S, the potential temperature of the surface water is nearly constant at ∼0.5 °C and the samples are in accord with the temperature trend established by surface seawater collected further to the north. However, at 64.2°S there is a small but well-resolved drop in potential temperature. It is likely that these two groups of samples (north and south of 64.2°S; Fig. 2) reflect the eastward and westward flowing limb of the Weddell Gyre, respectively (Klunder et al., 2011). This interpretation is corroborated by nutrient (NO$_3^-$, PO$_4^{3-}$, Si) data, which also fall in two groups that encompass the same latitudes. In detail, [NO$_3^-$], [PO$_4^{3-}$], and [Si] decrease southwards in the Weddell Gyre until about 65°S, but even further to the south, the parameters first increase and then decrease in southward direction (Fig. 2). The decrease south of ∼67.5°S is probably related to an earlier (December 2007) algae bloom, which followed the retracting ice edge with a time lag (Rutgers van der Loeff et al., 2011).
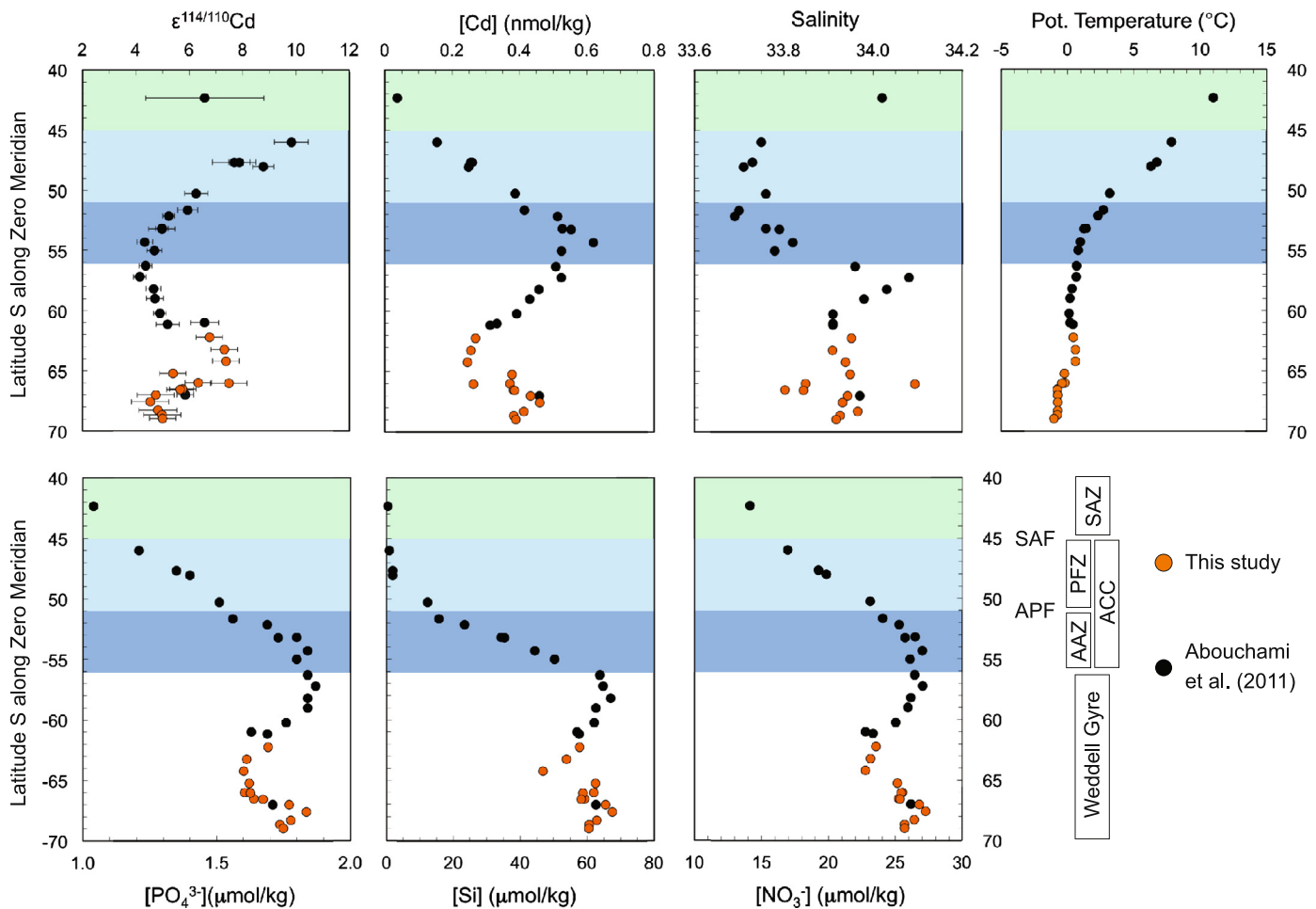
Fig. 2. The Cd concentrations and isotopic compositions, as well as hydrographic and nutrient concentration data are shown as a function of latitude for the Zero Meridian surface water samples of this study and Abouchami et al. (2011). Most noteworthy is how well the Cd data of Abouchami et al. (2011) for the surface water sample from Station 163 at ~66°S matches with the Cd results of the present study for neighboring locations. SAZ = Subantarctic Zone, PFZ = Polar Frontal Zone, AAZ = Antarctic Zone, ACC = Antarctic Circumpolar Current, SAF = Subantarctic Front, APF = Antarctic Polar Front. Note the strong gradient versus latitude for [Si], which is strongly depleted in the PFZ whilst [PO_4^{3-}] and [NO_3^-] are high. Only the AAZ and Weddell Gyre are thus truly HNLC for all three major nutrients.

4.2. Cd concentrations and isotope compositions of Zero Meridian surface seawater

The Cd concentrations and isotope compositions of the Zero Meridian surface seawater from this investigation and Abouchami et al. (2011) are also shown in Fig. 2. A key observation is that the data of the two studies match perfectly, with no apparent offsets in the results. This conclusion is in accord with previous work by the two laboratories, which demonstrated excellent agreement in the Cd data for both isotope reference materials (Abouchami et al., 2012) and GEOTRACES seawater intercomparison samples (Boyle et al., 2012) These observations are important, because they allow the Cd datasets of both studies to be interpreted in unison, with no need to correct for systematic differences in the results.

Focusing on the surface waters analyzed here, the Weddell Gyre transect displays Cd concentrations of 0.25 nmol/kg to 0.46 nmol/kg and $\varepsilon^{114/110}$Cd values between about +4.5 and +7.5 (Fig. 2, Table 1). Importantly, these data can be used to divide the samples into the same two regional groups (north and south of ~65°S) that were previously identified based on potential temperature and major nutrients.
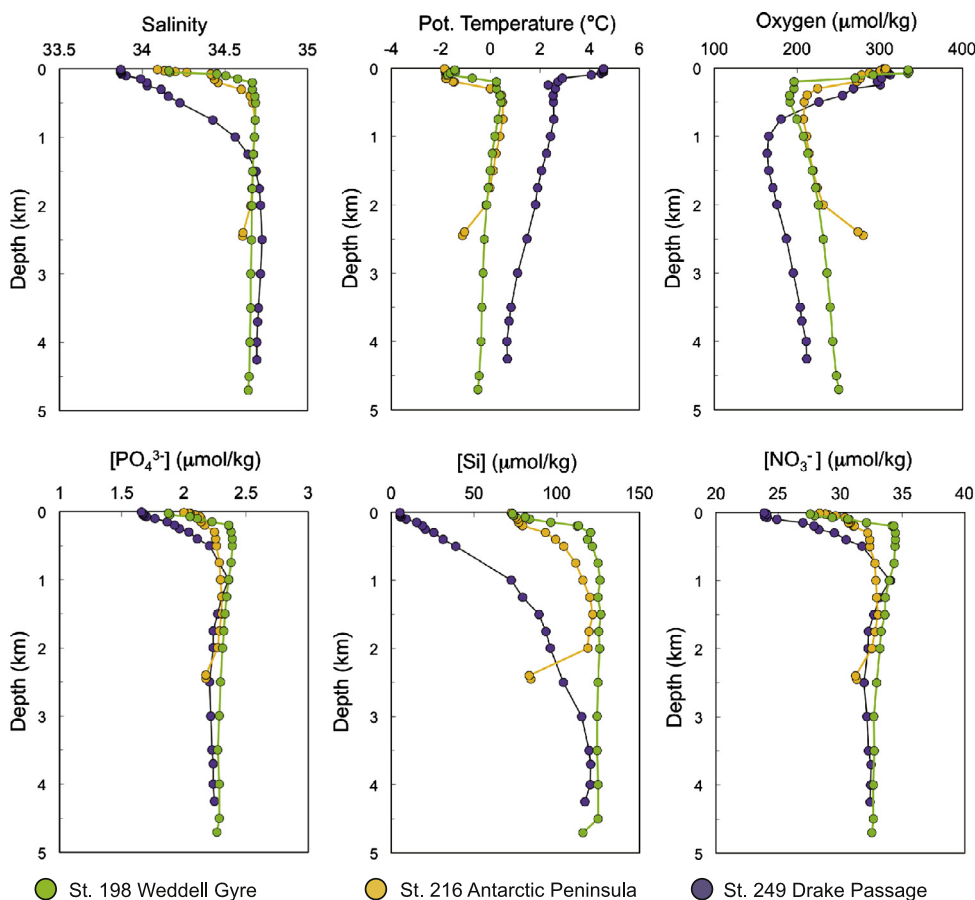
4.3. Hydrography and nutrient concentrations for the depth profiles

The hydrographic and nutrient data for the three depth profiles are summarized in Fig. 3. The most apparent feature is the similar-ity of the results obtained for Stations 198 and 216, whilst Station 249 from the Drake Passage differs in its physical and chemical properties. This result is not surprising given that the two former stations are within the Weddell Gyre (Fig. 1), whilst the latter is situated in the PFZ of the ACC system (Middag et al., 2012) with its distinct hydrographic and chemical characteristics (e.g., Löscher et al., 1998; Sarmiento et al., 2004; Middag et al., 2011; Abouchami et al., 2011). Stations 198 and 216 show temperature minima near the surface due to the presence of AASW, whilst Station 249 records a surface water temperature maximum from inflow of warmer waters into the PFZ. Notably, Station 249 exhibits much lower [Si] than the Weddell Gyre (Stations 198, 216), particularly at or near the surface (Fig. 3). In contrast, the depth profiles of all three stations reveal that [PO_4^{3-}] and [NO_3^-] are modestly depleted in the surface waters, whereby this depletion is slightly more pronounced in the Drake Passage (Station 249). Also conspicuous are the data for the deepest waters of Station 216 (Fig. 3; Table 1). These samples were collected just above the shelf of the Antarctic Peninsula and they feature temperatures more akin to the surface than the overlying waters, high O_2 contents, as well as low concentrations of [Si] and to a lesser extent other nutrients.

4.4. Cd concentrations and isotope compositions for the depth profiles

The depth profiles of Cd concentrations and isotope compositions are relatively similar for all three stations (Fig. 4, Ta-

Fig. 3. Depth profiles of hydrographic data and nutrient concentrations for Station 198 in the Weddell Gyre, Station 216 in the vicinity of the Antarctic Peninsula and Station 249 in the Drake Passage.
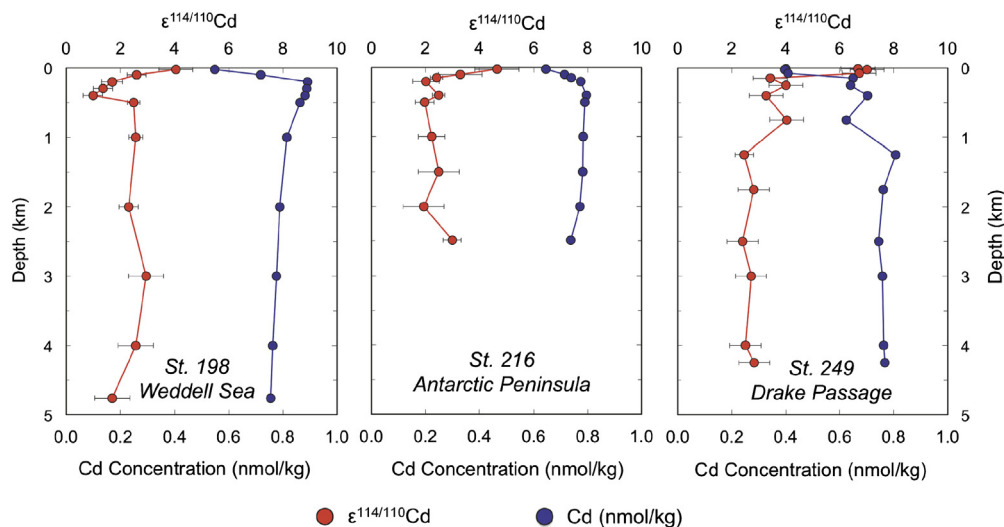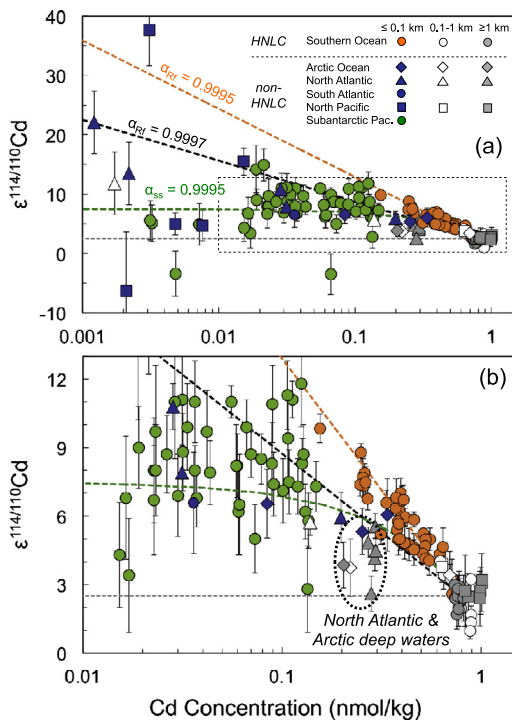

Fig. 4. Depth profiles of Cd isotope compositions (red dots; as $\varepsilon^{114/110}$Cd) and dissolved Cd concentrations (blue dots) for Stations 198 (Weddell Gyre), 216 (Antarctic Peninsula) and 249 (Drake Passage). (For interpretation of the references to color in this figure legend, the reader is referred to the web version of this article.)

ble 1), whereby Cd is modestly depleted in surface waters with concentrations ranging from ∼0.4 nmol/kg in the Drake Passage to ∼0.7 nmol/kg in the Weddell Gyre. These results are in accord with the only moderately fractionated $\varepsilon^{114/110}$Cd values of between +4.0 to +6.7. In addition, all depth profile samples from below 1 km feature nearly identical Cd concentrations and isotope compositions, whereby the largest deviation (with relatively low [Cd] and high $\varepsilon^{114/110}$Cd) is seen for 2450 m at

Station 216. Nonetheless, these data (and one additional published result; Ripperger et al., 2007) provide well-defined Southern Ocean deep water averages of [Cd] = 0.77 ± 0.01 nmol/kg and $\varepsilon^{114/110}$Cd = +2.5 ± 0.2 (2se, $n = 16$) for samples from depths >1000 m (see Supplement Section 5).

At depths of between about 200 m and 1 km there are clear differences in the Cd data for Station 249 versus Stations 198 and 216 (Fig. 4). Most notably, Station 249 reveals $\varepsilon^{114/110}$Cd values

Fig. 5. Plots of Cd isotope compositions versus concentrations (note logarithmic scale for *x*-axis) for seawater from the Southern Ocean HNLC region and non-HNLC open ocean areas. Samples from depths $\leqslant 100$ m are highlighted in color whilst waters from depths $\geqslant 1$ km are shown in gray. Shown for reference are different calculated isotope fractionation trends for dissolved seawater Cd from biological uptake (dashed lines). The large scale of panel (a) shows all published data, whilst panel (b) highlights the results obtained for samples with higher Cd concentrations and $\varepsilon^{114/110}$Cd of between 0 and +13. (a) The shallow Southern Ocean samples (in orange) define a coherent but broad trend within the scatter of the global data for samples from $\leqslant 100$ m, including data from a recent regional study in the Subantarctic Pacific (Pac.; green symbols). Changes in the conditions of biological Cd uptake and associated isotope fractionation will be responsible for a substantial part of this scatter. For example, different fractionation trends are generated by (i) variable fractionation factors α, (ii) variable conditions that induce changes between closed system Rayleigh fractionation (α_{Rf}) and steady state isotope fractionation in an open system (α_{ss}), or different initial water mass compositions. (b) This panel highlights that some deep water samples from the Atlantic and Arctic Ocean have higher $\varepsilon^{114/110}$Cd values than deep water from the Southern and Pacific Ocean. Data sources: Ripperger et al. (2007) (N. Pacific, Arctic, Atlantic Ocean); Abouchami et al. (2011) (Southern Ocean, S. Atlantic); Xue et al. (2012) (N. Atlantic); Gault-Ringold et al. (2012) (Subantarctic Pacific); this study (Southern Ocean). (For interpretation of the references to color in this figure legend, the reader is referred to the web version of this article.)

the largest variability of Cd concentrations and isotope compositions. The new HNLC data are hence in accord with earlier studies, which concluded that biological cycling of Cd is the main process responsible for generating variations in seawater $\varepsilon^{114/110}$Cd (Lacan et al., 2006; Ripperger et al., 2007; Abouchami et al., 2011; Gault-Ringold et al., 2012; Horner et al., 2013).
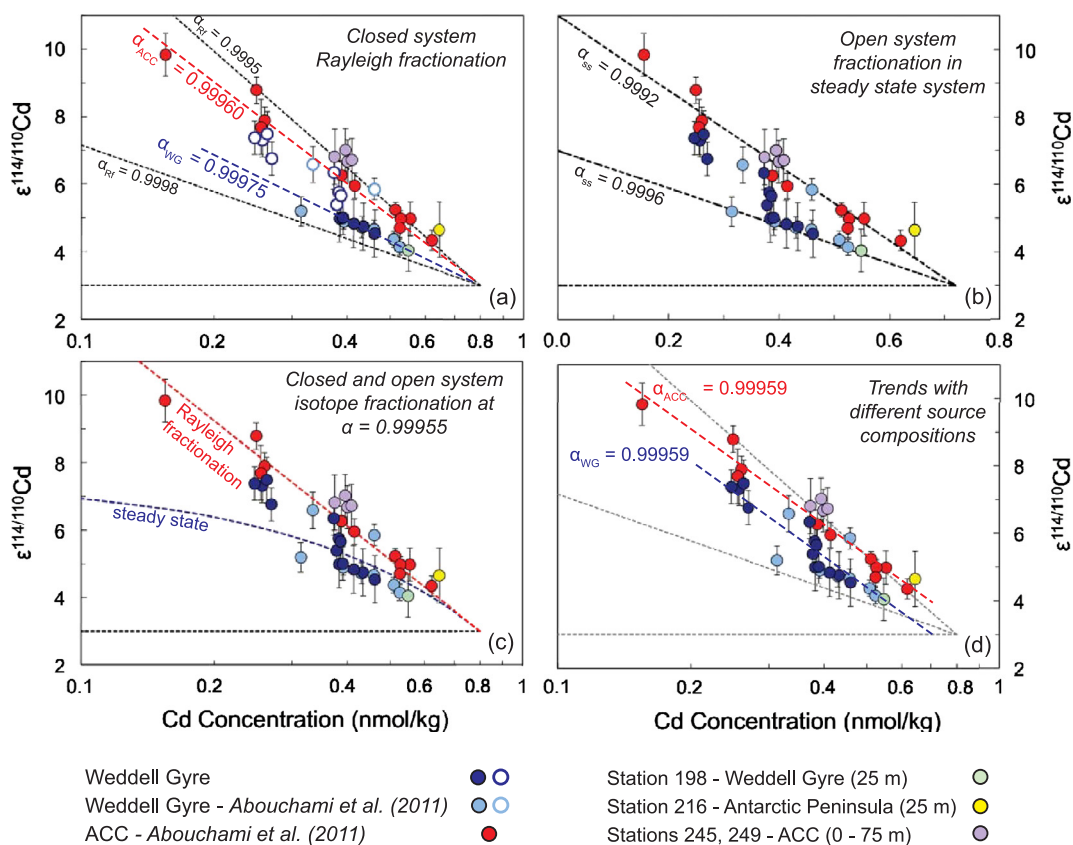
Fig. 5 furthermore confirms that surface and near-surface seawater from the HNLC ocean features relatively high Cd contents and, therefore, can be readily distinguished from non-HNLC locations. To a lesser extent, such a distinction is also possible based on Cd isotope compositions. The shallow non-HNLC ocean shows significant isotopic variability, particularly at low [Cd] with $\varepsilon^{114/110}$Cd values from about −5 to +40. In contrast, the HNLC samples feature much less isotopic variability with Cd isotope effects that rarely exceed $\varepsilon^{114/110}$Cd $\approx +8$. Assuming that Cd isotope fractionation results from biological cycling, the modest range of $\varepsilon^{114/110}$Cd in the HNLC ocean is consistent with the low productivity of these regions and the limited uptake of Cd by phytoplankton.

Fig. 5 also highlights that the HNLC surface and subsurface samples ($\leqslant 100$ m depth; orange symbols) define a comparatively tight trend, in comparison to the large global variability of Cd data in similar samples from other locations. This observation holds even when our results for a single growing season are compared with data from the only previous regional study of marine Cd isotope variations (Gault-Ringold et al., 2012), which investigated Subantarctic surface waters that were collected on a ∼100 km long transect, albeit over a two year period (Fig. 5; green symbols). The variability of the global data reflects that the samples are from a range of biogeochemical regimes, such that they record both different conditions of Cd uptake and a myriad of other processes that can impact Cd systematics, including mixing of isotopically distinct water masses, external inputs of Cd (e.g., from aerosol), and remineralization of organic matter. The isotopic trends that are generated by biological uptake can also differ in response to a number of variables. For example, correlations with distinct slopes can be generated in Fig. 5 for different values of the biological fractionation factor α, where $\alpha = R_{\text{biomass}}/R_{\text{seawater}}$ and $R = {}^{114}$Cd$/{}^{110}$Cd (Fig. 5a). Further variability can be produced even when α is constant, if Cd uptake occurs at conditions that fluctuate between the endmember cases of closed system Rayleigh fractionation (α_{Rf}) and steady state isotope fractionation in an open system (α_{ss}; Fig. 5a).

Given the multiple factors that can impact marine Cd systematics it is not surprising that the global data for surface seawater collected at different times and locations exhibits such large variability in Fig. 5. In contrast, the comparatively tight 'HNLC trend' of the Southern Ocean surface and subsurface seawater thus reflects a comparatively uniform history of marine conditions and biogeochemical processes that impact Cd cycling, even though the samples were collected over a large region during a period of nearly 2 months (Fig. 1).

5.2. Biological Cd isotope fractionation in the Southern Ocean

Fig. 6 focuses only on the Cd data available for samples from the upper mixed layer of the Southern Ocean. This comprises the surface waters from the 'Zero Meridian' transect and samples from the surface mixed layer (Rutgers van der Loeff et al., 2011) of Stations 198 (25 m depth), 216 (25 m), 245 (2–5 m) and 249 (25, 50, 75 m). These graphs confirm the previously inferred Southern Ocean 'HNLC trend', but also reveal significant fine structure (and/or scatter) within the correlation. In particular, it is apparent that the ACC samples typically feature slightly higher $\varepsilon^{114/110}$Cd values at a given [Cd] compared to the Weddell Gyre surface waters. The upper mixed layer samples from the Drake Passage (Stations 245, 249) and Station 198 support this conclusion, with Cd systematics akin to those of the ACC and Weddell Gyre surface

of about +4 at depths of 150 to 750 m, and this coincides with relatively constant [Cd] and potential temperatures (Fig. 3). In contrast, Cd concentrations at Stations 198 and 216 increase rapidly from the surface to maximum values of about 0.89 nmol/kg at 200–400 m depth. Notably, this [Cd] maximum coincides with unusually low $\varepsilon^{114/110}$Cd values of about +1 to +2.

5. Discussion

5.1. Cd isotope variations in the upper water column – comparison of the Southern Ocean HNLC region with the global ocean

In Fig. 5, the data obtained here and by Abouchami et al. (2011) for HNLC seawater from the ACC and Weddell Gyre are compared with previously published results for seawater samples from non-HNLC locations in a plot of $\varepsilon^{114/110}$Cd versus the natural logarithm of Cd concentration. The most obvious feature of Fig. 5 is that data for both HNLC and non-HNLC samples from shallow depths of $\leqslant 100$ m, where biological activity is prevalent, show by far

Fig. 6. Diagrams of $\varepsilon^{114/110}$Cd versus Cd concentrations for Zero Meridian surface seawater and mixed layer samples from additional stations. Note logarithmic scale of x-axis in (a), (c), (d) and linear scale in (b). The dashed lines denote various isotope fractionation trends for dissolved seawater Cd that are distinguished by distinct values of the fractionation factor α. Calculated (as opposed to fitted) fractionation trends apply source compositions in accord with data for this region, with $\varepsilon^{114/110}$Cd $= +3.0$ and Cd contents of either 0.72 (b) or 0.80 nmol/kg (a, c, d) to obtain visually optimized fits. (a) The calculated Rayleigh fractionation lines indicate that the observed broad 'HNLC trend' is in accord with closed system Rayleigh fractionation. The bold colored lines are the distinct fractionation trends that were assigned by Abouchami et al. (2011) to their data for the ACC (α_{ACC}; red symbols) and the Weddell Gyre (α_{WG}; light blue symbols). Denoted by open symbols are Weddell Gyre samples that do not fall on the respective trend. (b) The Southern Ocean data are also in accord with linear fractionation trends, as expected for open system steady state isotope fractionation, albeit using different α values. (c) The scatter within the 'HNLC trend' can, in principle, be explained by fractionation conditions that vary between the endmember scenarios of closed system Rayleigh fractionation and open system fractionation at steady state. (d) The bold colored lines denote the two essentially parallel trends that were obtained by fitting lines separately to the ACC and the Weddell Gyre (WG) data. The boundary between these two regimes was drawn at 56°S (see text and Supplement Section 4). (For interpretation of the references to color in this figure legend, the reader is referred to the web version of this article.)

samples, respectively (Fig. 6). In the following, we investigate the systematic nature of the Cd data within the HNLC trend and, using simple modeling, assess possible causes for its features. In particular, the discussion focuses on (i) variable fractionation factors, (ii) changes in the fractionation conditions, and (iii) differences in source water compositions.

5.2.1. Variable apparent fractionation factors

Previously, Abouchami et al. (2011) concluded that their Southern Ocean samples defined two linear correlations in a plot of $\varepsilon^{114/110}$Cd versus ln([Cd]), implying two distinct values of α (Fig. 6a). In detail, they found that samples from ACC locations between 46°S and 56°S define a correlation with a slope equivalent to a fractionation factor of $\alpha_{ACC} = 0.99960$, whilst most samples from 56°S to 61°S in the Weddell Gyre are in accord with a less steep trend indicative of $\alpha_{WG} = 0.99975$ (Fig. 6a, red and blue dashed lines). Abouchami et al. (2011) inferred that the Cd systematics of these samples are in accord with biological isotope fractionation in two regimes that are associated with distinct values of α, as a consequence of differences in phytoplankton biomass, community composition, and/or physiological mechanisms of Cd uptake (see Supplement Section 3).

Combination of the present data with those of Abouchami et al. (2011) reveals that 7 of the new mixed layer samples from south of 56°S are in accord with the Weddell Gyre trend, whilst the

Drake Passage samples support the previous ACC correlation. However, Abouchami et al. (2011) also observed that two of their Weddell Gyre samples did not conform to the expected trend (open light blue symbols; Fig. 6a) and even more "scatter" is added by samples from the present study (open dark blue symbols; Fig. 6a). These deviations from the predicted closed system Rayleigh fractionation trends may reflect atypical conditions at the respective locations, which are associated with distinct or intermediate fractionation factors. For example, three of the present samples from the Weddell Gyre, located between 60° and 65°S fall along the ACC correlation. Such a shift to heavier $\varepsilon^{114/110}$Cd values was also noted by Abouchami et al. (2011) for one of their samples from this region and thought to be related to an earlier phytoplankton bloom in December 2007 (see Supplement Section 3). The Weddell Gyre samples from around 66°S plot between the ACC and Weddell Gyre trends of Fig. 6a and they also show unusual contrasting changes in $\varepsilon^{114/110}$Cd and [Cd] (Fig. 2). It is conceivable that these features reflect the influence of melt water from icebergs, an explanation that has also been put forward for the variable Fe concentrations in this region (Klunder et al., 2011).

5.2.2. Closed versus open system fractionation – variable 'conditions' of Cd uptake and isotope fractionation

Figs. 6a/b show that the Southern Ocean mixed layer samples are in accord with linear $\varepsilon^{114/110}$Cd versus [Cd] trends regardless

of whether the concentrations are plotted in ln([Cd]) or [Cd] space. This indicates that the correlations are, in principle, compatible with both closed system Rayleigh fractionation (Fig. 6a) and open system isotope fractionation in a steady state system (Fig. 6b). The compatibility of the data with both endmember models of isotope fractionation reflects, at least in part, the comparatively modest depletion of Cd in HNLC surface waters compared with the global ocean dataset (Fig. 5). A clear isotopic distinction between the models is only seen at low Cd contents, but such conditions are not observed in the Southern Ocean.

A key difference between the two scenarios is that an open, steady state system requires a larger isotope fractionation factor (i.e., smaller value of α) to account for the correlations seen in Fig. 6b, in comparison to the closed system model of Fig. 6a. Using similar and realistic source compositions (see caption of Fig. 6), steady state fractionation can span the Cd data with $\alpha_{ss} \approx 0.9996$ to 0.9992 (hashed lines; Fig. 6b), whilst α_{Rf} values between 0.9998 and 0.9995 are required to completely cover the results for closed system Rayleigh fractionation (black dashed lines, Fig. 6a). The modeling of Fig. 6c demonstrates that the total variability of the mixed layer Cd data can, in principle, be explained with a single fractionation factor of $\alpha = 0.99955$, only by changing the conditions between the endmember scenarios of steady state and Rayleigh fractionation. Whilst it is unclear whether such a scenario is realistic, as it requires large and highly localized variations between open and closed system fractionation to explain the Weddell Sea 'outliers', the result is nonetheless instructive because it demonstrates that such variations can strongly impact Cd cycling in the upper water column.

Changes in 'fractionation conditions' that may vary between the endmember conditions defined by the closed and open system scenarios will be driven by processes that alter the rate of biological Cd uptake relative to Cd replenishment in the water column. In the mixed layer, Cd is primarily replenished by remineralization of biomass and water mass mixing, thereby supporting open system conditions. The Weddell Gyre appears to feature more pronounced subsurface Cd enrichments from remineralization than the ACC (see Section 5.3.2) and upwelling of nutrient-rich CDW is limited to regions south of the APF. Hence, the gentler slope of the Weddell Gyre correlation compared to the ACC (Fig. 6) may reflect conditions that are more favorable for open system fractionation. In contrast, transient phytoplankton blooms will generate high rates of Cd removal and can therefore act to generate temporary shifts in the apparent 'openness' of a system toward more Rayleigh-like (closed system) conditions. The bloom observed between 60° to 65°S in December 2007 is, therefore, consistent with the unusually high $\varepsilon^{114/110}$Cd values for the Weddell Gyre samples from this area.

5.2.3. Differences in source water compositions

It is also possible that the variability of the mixed layer Cd data (Fig. 6) is a consequence of differences in source water compositions. This scenario is discussed in the following based on statistical tests (Supplement Section 4) that were applied to all mixed layer results with the exception of Station 216, which may be affected by the proximal shelf. Seawater from the Drake Passage and transect samples from north of 56°S were hereby assigned to the ACC regime ($n = 15$) and more southern samples to the Weddell Gyre ($n = 22$), in accord with the division adopted in earlier studies of samples from the same cruise (e.g., Abouchami et al., 2011; Middag et al., 2011; Klunder et al., 2011).

The statistical assessment pertains to data plotted in $\varepsilon^{114/110}$Cd versus ln([Cd]) space, which assumes Rayleigh distillation (Fig. 6d), but very similar results were obtained for a linear plot and a steady state system (Supplement Section 4). The complete dataset defines a slope of $\alpha_{Rf} = 0.99959 \pm 0.00008$ (all uncertainties are

±2sd), but separating the data into an ACC and Weddell Gyre trend, based on the division outlined above, provides a statistically significant improvement in fit ($p = 1 \times 10^{-7}$). These two trends (Fig. 6d, dashed lines) have identical slopes, corresponding to fractionation factors of $\alpha_{ACC} = 0.99959 \pm 0.00005$ and $\alpha_{WG} = 0.99959 \pm 0.00009$, but they are offset by $\varepsilon^{114/110}$Cd $= 1.1$. This suggests that the Cd data are in accord with assignment of the samples into two different groups – as in Abouchami et al. (2011) – albeit with identical slopes (or apparent α's). The small but significant offset between the two trends can be explained by a difference in the Cd isotope composition of the source water masses and this may reflect larger fluxes of isotopically light Cd into Weddell Gyre source waters from the remineralization of biomass or perhaps upwelling of water with more positive $\varepsilon^{114/110}$Cd in the ACC region.

5.2.4. Synthesis

Biological cycling of Cd in the mixed layer of the Southern Ocean results in a co-variation of dissolved $\varepsilon^{114/110}$Cd with [Cd]. Detailed assessment reveals significant fine structure within the 'HNLC trend', which is most likely caused by either changes in the biological fractionation factor (Abouchami et al., 2011), variable 'fractionation conditions' (closed versus open system) and/or distinct compositions for the source water masses. A better understanding of the relative importance of these factors in determining the Cd systematics seen in Fig. 6 is desirable, as this would provide new insights into the processes that govern the dynamic cycling of Cd in the upper water column.

In principle, the relative impact of changes induced by variable fractionation factors and/or conditions could be assessed based on independent estimates of α from culturing experiments, but only scant data are currently available. Experiments with freshwater chlorophytes provide a fractionation factor of 0.9986 ± 0.0006 (Lacan et al., 2006), whereas the 'accidental' growth of phytoplankton in unfiltered seawater (Xue et al., 2012) and experiments with genetically modified bacteria (Horner et al., 2013) yielded estimates of 0.9995 ± 0.003 and ~ 0.9997, respectively. Perhaps most relevant for the Southern Ocean are the data of Gault-Ringold (2011) for cultured diatoms grown under Zn-limited and Zn-replete conditions, and these give α values of 0.9996 ± 0.0001 and 0.9991 ± 0.0001, respectively. Notably, the results of all studies are in good agreement with the fractionation factors that can be inferred from the Southern Ocean seawater trends (Fig. 6). Given that culturing experiments can never reproduce, but only approximate, actual marine conditions, the current data provide insufficient constraints to rule out any of the scenarios for the origin of the variable Cd isotope systematics seen in Fig. 6. Hence, it is possible that either of these variables dominates the Cd systematics or they could be determined by a combination of factors.

The different Cd fractionation patterns seen in the ACC and Weddell Gyre by Abouchami et al. (2011) were inferred to reflect two distinct marine biogeochemical provinces, whereby atypical conditions in some regions are responsible for samples with unusual compositions (Fig. 6). Our results suggest an alternative interpretation. When considered in a global marine context, the mixed layer samples from the Southern Ocean display a tightly clustered trend (Fig. 5), and the Southern Ocean as a whole hence appears to offer comparatively homogeneous conditions of Cd cycling. Within this domain, the trends shown by the majority of the ACC and Weddell Gyre samples denote the overall variability of the processes and conditions that impact the cycling of Cd (Fig. 6). The heavier Cd isotope compositions seen in the ACC compared to the Weddell Gyre may represent more positive $\varepsilon^{114/110}$Cd source waters in the ACC, the expression of smaller α values (that generate larger fractionations) during Cd uptake and/or 'fractionation conditions' that are closer to idealized closed system Rayleigh dis-

tillation. Samples that are intermediate to these two endmembers, particularly from the Weddell Gyre, can thus be explained in terms of intermediate marine conditions that produce transitional fractionation signatures.

Based on our assessment, it will be useful for future studies to characterize the biological fractionation factor for Cd at conditions that are relevant for the surface ocean. Also important are investigations that constrain the effect of nutrients on marine Cd fractionation systematics. Such an impact is expected, given that a number of studies have reported that the uptake of Cd by phytoplankton is affected by ambient carbon dioxide concentrations, and the dissolved seawater contents of Cd, Fe, Zn and Mn (Lee et al., 1995; Sunda and Huntsman, 1998, 2000; Cullen et al., 1999, 2003; Cullen and Sherrell, 2005; Cullen, 2006; Lane et al., 2009).

5.3. Depth profiles

5.3.1. Deep water

The increasing Cd concentrations seen along the deepwater pathways of the meridional overturning circulation from the North Atlantic/Arctic Ocean, to the Southern Ocean and the Pacific are discernible in Fig. 5b. Our new data also supports previous work, which concluded that deep waters show only limited variability in Cd isotope compositions (Ripperger et al., 2007). Including the results of the present study, the new global dataset for seawater from depths $\geqslant 1$ km exhibits a mean $\varepsilon^{114/110}$Cd of $+3.0 \pm 0.3$ (2se, $n = 27$; see Supplement Section 5).

Fig. 5b highlights that the highest $\varepsilon^{114/110}$Cd values for deep water, of up to about $+5$, are found in samples from the Arctic and North Atlantic Ocean. Excluding these values, the compilation of Southern and Pacific Ocean deep waters have a marginally lower mean $\varepsilon^{114/110}$Cd $= 2.6 \pm 0.2$ (2se, $n = 21$; Supplement Section 5). Further data are, however, required to ascertain if there is a small systematic $\varepsilon^{114/110}$Cd offset between Arctic/North Atlantic and Southern/Pacific Ocean deep water masses. If confirmed, the more positive $\varepsilon^{114/110}$Cd values found in the former may represent a residual fractionated surface signal that is retained, along with low preformed [Cd], due to the young ventilation age of these water masses.

5.3.2. Stations 198 and 216 in the Weddell Gyre

Seawater from 200 m to 400 m depth at Station 198 in the Weddell Gyre demonstrates $\varepsilon^{114/110}$Cd values as low as about $+1$ (Fig. 4). A similar signature also appears to be present at Station 216 but this is less well resolved as the lowest $\varepsilon^{114/110}$Cd value is $+2$. It is unlikely that these light Cd isotope compositions are related to upwelling of CDW, the deep water source of Cd to the study sites, because all deep waters analyzed here display $\varepsilon^{114/110}$Cd values of higher than $+2$. The upwelling can, however, account for the nearly constant $\varepsilon^{114/110}$Cd $\approx +2.5$, which is observed for depths $\geqslant 500$ m at Station 198. Significantly, the lightest Cd isotope compositions for Stations 198 and 216 are recorded at approximately the same depths that show the highest [Cd]. This suggests that the low $\varepsilon^{114/110}$Cd values reflect addition of isotopically light Cd, most likely from remineralization of organic matter. Mass balance modeling (Fig. 7a) is used in the following to support this conclusion.

The green lines of Fig. 7a indicate the calculated isotopic evolution for Cd that is accumulated in biomass by biological uptake. These calculations are for both closed system Rayleigh fractionation and for an open, steady state system using small but reasonable values for α to maximize the extent of fractionation ($\alpha_{Rf} = 0.9996$ and $\alpha_{ss} = 0.9994$) and a realistic initial seawater composition ($\varepsilon^{114/110}$Cd $= +2.5$, [Cd] $= 0.8$ nmol/kg). The modeling shows that biomass with isotopically light Cd is likely to be
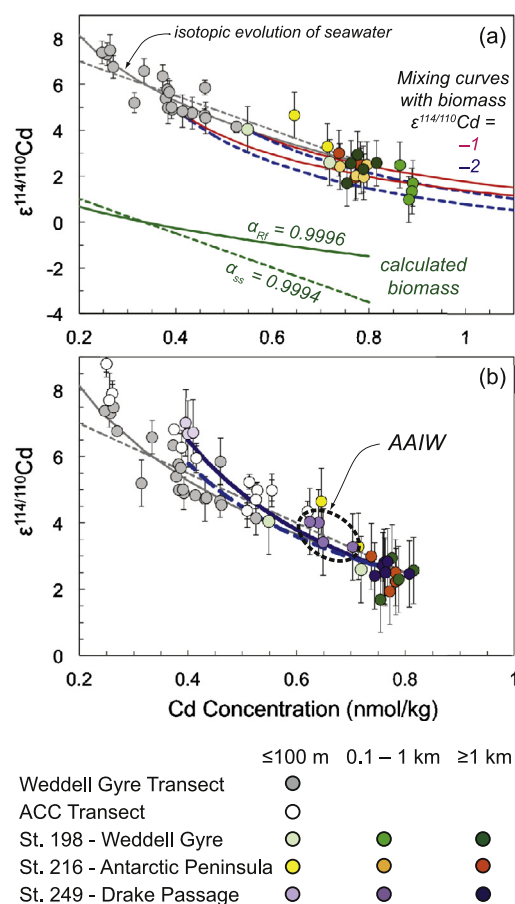
Fig. 7. Cadmium isotope compositions versus Cd concentrations for selected (see below) Southern Ocean seawater samples. For reference, the thin gray lines denote the dissolved seawater Cd trends calculated for biological uptake of Cd and associated (i) closed system Rayleigh fractionation at $\alpha_{Rf} = 0.9996$ (full lines) and (ii) steady state isotope fractionation at $\alpha_{ss} = 0.9994$ (dashed lines). (a) For clarity, only data for Weddell Gyre surface water and profiles are shown. The green lines record the Cd isotope composition of the corresponding accumulated biomass that is generated at a given degree of Cd depletion in seawater. Remineralization of such biomass and mixing with surface seawater can explain that $\varepsilon^{114/110}$Cd values as low as $+1$ and high [Cd] are observed at intermediate depth at Station 198. This is illustrated by the trends calculated for remineralization of biomass characterized by $\varepsilon^{114/110}$Cd values of -1 (full red lines) and -2 (dashed blue lines) and addition to two surface seawater compositions that are reasonable for the Weddell Gyre, with [Cd] = 0.40 and 0.55 nmol/kg, $\varepsilon^{114/110}$Cd = +4.9 and +4.0, respectively. (b) In this panel, data from intermediate depths (0.1 to 1 km) in the Weddell Gyre is omitted. The two blue trends (full and dashed lines) show that mixing of Southern Ocean surface waters (with [Cd] = 0.40 nmol/kg and $\varepsilon^{114/110}$Cd = 5.8 and 6.5) with a deep water composition ([Cd] = 0.75 nmol/kg, $\varepsilon^{114/110}$Cd = +2.7) can account for the Cd systematics observed for the Station 249 (Drake Passage) intermediate depth (150 to 750 m) water masses that are inferred to be AAIW. (For interpretation of the references to color in this figure legend, the reader is referred to the web version of this article.)

common in HNLC regions where Cd uptake is incomplete. In detail, the accumulated biomass features $\varepsilon^{114/110}$Cd $\leqslant 0$, if the residual dissolved seawater Cd concentration (following biological removal) exceeds 0.3 nmol/kg, in accord with the majority of the Weddell Gyre surface waters (Fig. 7a).

Fig. 7a also shows the mixing curves (in red and blue) that are generated by addition of Cd released from biomass to typical Southern Ocean surface waters, whereby the latter are the starting points of the mixing trends at low [Cd]. The biomass is assigned a Cd abundance of 2×10^4 nmol/kg, in accord with published elemental data for diatoms and other phytoplankton (Price, 2005; Ho et al., 2003; Supplement Section 6), but the exact value of this parameter is of little consequence because essentially identical results are obtained for Cd contents of 10^2 to 10^6 nmol/kg.

For biomass characterized by $\varepsilon^{114/110}$Cd $= -1.0$, a value that is in accord with both Rayleigh and steady state fractionation, remineralization can produce $\varepsilon^{114/110}$Cd values as low as $+1.5$ for seawater with [Cd] ≈ 0.9 nmol/kg, as observed for Stations 198 and 216 at depths of 200 to 400 m (full red lines, Fig. 7a).

The model described above cannot, however, account for $\varepsilon^{114/110}$Cd values of less than $+1.4$, as observed for two samples from Station 198. For remineralization to produce seawater with $\varepsilon^{114/110}$Cd $\approx +1$ at [Cd] ≈ 0.9 nmol/kg, the biomass must feature $\varepsilon^{114/110}$Cd of about -2 or less (dashed blue lines, Fig. 7a). Given the constraints of the seawater data on the fractionation factor α (Fig. 6), such biomass can only be produced by isotope fractionation in an open or at least partially open system, rather than by Rayleigh distillation (Fig. 7a). This conclusion is in accord with the observation that the majority of the Weddell Gyre surface waters are offset to lower $\varepsilon^{114/110}$Cd values in comparison to the ACC trend (Fig. 6).

The possible role of remineralization can be further evaluated by incorporating the C budget into the modeling. Assuming that the biomass is characterized by a molar C/Cd ratio of 3.3×10^5 (Price, 2005; Ho et al., 2003; Supplement Section 6), the extent of remineralization that is needed to account for the Cd-rich water samples with $\varepsilon^{114/110}$Cd $\approx +1$ at Station 198 would increase the concentration of dissolved inorganic carbon (DIC) by about 150 to 250 µmol/kg, equivalent to an increase of about 5 to 10%. Given the uncertainties of the mass balance, this prediction is in accord with the observation that Station 198 samples from 200 to 400 m depth feature DIC contents, which exceed the surface concentrations by about 90 µmol/kg (Supplement Section 1). In summary, the modeling demonstrates that the addition of remineralized Cd, which records incomplete nutrient utilization at the surface, provides a reasonable explanation for the low $\varepsilon^{114/110}$Cd values and high Cd contents seen at 200 to 400 m depth in the Weddell Sea.

Of further interest is the deepest sample from Station 216, obtained just above the shelf sediments of the Antarctic Peninsula at 2450 m, which features conspicuous hydrographic and nutrient data (Fig. 3). Based on these and other observations (e.g., elevated [Mn] and [Al]), Middag et al. (2013) concluded that freshly ventilated deep waters are being sampled at this location, which formed close to the shelf by cooling, brine rejection and subsequent subduction. The low Cd concentration and hint of higher $\varepsilon^{114/110}$Cd for the 2450 m sample (Fig. 4, Table 1) are in accord with the conclusion of Middag et al. (2013) and hence indicate that the fractionated Cd isotope signatures of surface waters can be subducted into and retained within the deep ocean.

5.3.3. Station 249 in the Drake Passage

Nearly constant $\varepsilon^{114/110}$Cd values of about $+4$ were found for seawater from depths of 150 to 750 m at Station 249 in the Drake Passage (Fig. 4). This result is of interest because such positive and relatively constant $\varepsilon^{114/110}$Cd values were not detected at similar depths in any previous study and it is conceivable that they are also a residual signal from isotope fractionation at the surface.

Based on the hydrographic data of the cruise (Table 1), Station 249 is clearly within the PFZ (Middag et al., 2012). These results are also in accord with studies of physical oceanography, which have shown that AAIW is present within the PFZ below the mixed layer, centered on a depth of about 500 m (Santoso and England, 2004; Carter et al., 2009; Naveira Garabato et al., 2009; Sudre et al., 2011). Whilst some nutrient data (particularly negative Si*; Supplement Section 1) may also hint at the presence of SAMW in the upper 150 to 250 m of Station 249, the water mass studies generally conclude that SAMW overlies AAIW only to the north of the SAF. Based on these considerations, the main water mass for Station 249 at 150 to 750 m depth is thus freshly ventilated AAIW, which is characterized by $\varepsilon^{114/110}$Cd $\approx$ $+4$ and [Cd] ≈ 0.65 nmol/kg. This conclusion is corroborated by previous investigations, which have observed fractionated N and Si isotope signatures for AAIW (and SAMW; Rafter et al., 2012; de Souza et al., 2012) and further supported by simple modeling (Fig. 7b), as discussed below.

A number of previous studies have shown that AAIW is formed by subduction of surface/mixed layer waters, with a chemical signature that is subsequently modified by mixing processes (e.g., Sievers and Nowlin, 1984; Santoso and England, 2004). The slightly fractionated Cd isotope composition of AAIW is thus most likely a consequence of biological fractionation near the surface and moderation of this signal by mixing. Such a scenario is confirmed by calculations, which demonstrate (Fig. 7b) that the Cd composition inferred for AAIW can be obtained as a mixture of Weddell Gyre or ACC surface waters (although AAIW at Station 249 is sourced eastward of the Drake Passage; Naveira Garabato, 2009) and Southern Ocean deep water (from $\geqslant 1$ km depth). Given that our results show that a fractionated Cd isotope surface signature can be preserved at depth to a sufficient extent to be still recognizable in AAIW, it will be of interest for future studies to determine how far northward this isotopic signal is retained along the water mass flowpath.

6. Conclusions

The new Cd concentration and stable isotope data for surface seawater and three depth profiles from the Southern Ocean provide a number of important observations and interpretations:

(1) The data of this study and Abouchami et al. (2011) for seawater from the upper mixed layer define a broad but clear 'HNLC trend' in a plot of $\varepsilon^{114/110}$Cd versus [Cd], which is primarily a consequence of isotopic fractionation associated with biological uptake. In comparison to surface water samples from non-HNLC locations, Southern Ocean surface water features relatively high Cd concentrations (typically from 0.2 to 0.6 nmol/kg) and only moderately fractionated $\varepsilon^{114/110}$Cd, generally between $+4$ and $+8$. These data reflect the limited biological productivity of the HNLC ocean. Detailed assessment reveals fine structure within the 'HNLC trend', which records differences in the biological fractionation factor, variable fractionation conditions (closed versus open system) or distinct compositions for the source water masses, or a combination of these factors.

(2) Southern Ocean seawater from depths $\geqslant 1$ km has an average $\varepsilon^{114/110}$Cd $= \pm 2.5 \pm 0.2$ (2se, $n = 16$). This agrees well with published Cd data and the combined global dataset supports a relatively uniform deep water Cd isotope composition, with an average $\varepsilon^{114/110}$Cd of $+3.0 \pm 0.3$ (2se, $n = 27$) for samples from depths $\geqslant 1$ km.

(3) Significant differences in Cd isotope compositions were observed for seawater from intermediate depths. Samples from 200 m to 400 m depth in the Weddell Gyre have $\varepsilon^{114/110}$Cd values as low as $+1$. These light isotope compositions most likely reflect the addition of remineralized Cd from biomass that records incomplete nutrient utilization at the surface. Samples from depths of 150 m to 750 m in the Drake Passage where AAIW is the dominant water mass, display relatively low [Cd] of ~ 0.65 nmol/kg and moderately fractionated $\varepsilon^{114/110}$Cd of about $+4$. This Cd signature of AAIW is a consequence of biological Cd isotope fractionation near the surface and moderation of the biological signal by mixing, in accord with the formation history of this water mass.

In summary, our results demonstrate that coupled Cd isotope and concentration data provide valuable new insights into the dis-

tribution and cycling of Cd in the ocean. The highly systematic nature of the Cd isotope signatures may furthermore prove to be of utility for future research in marine geochemistry and paleoceanography.

Acknowledgements

Appendix A. Supplementary material

Supplementary material related to this article can be found online at http://dx.doi.org/10.1016/j.epsl.2013.09.014.

References

Abouchami, W., Galer, S.J.G., de Baar, H.J.W., Alderkamp, A.C., Middag, R., Laan, P., Feldmann, H., Andreae, M.O., 2011. Modulation of the Southern Ocean cadmium isotope signature by ocean circulation and primary productivity. Earth Planet. Sci. Lett. 305, 83–91.

Abouchami, W., Galer, S.J.G., Horner, T.J., Rehkämper, M., Wombacher, F., Xue, Z., Lambelet, M., Gault-Ringold, M., Stirling, C.H., Schonbächler, M., Shiel, A.E., Weis, D., Holdship, P.F., 2012. A common reference material for cadmium isotope studies – NIST SRM 3108. Geostand. Geoanal. Res. 37, 5–17.

Boyle, E.A., Sclater, F., Edmond, J.M., 1976. On the marine geochemistry of cadmium. Nature 263, 42–44.

Boyle, E.A., John, S., Abouchami, W., Adkins, J.F., Echegoyen-Sanz, Y., Flegal, R., Fornace, K., Gallon, C., Galer, S., Gault-Ringold, M., Lacan, F., Radic, A., Rehkämper, M., Rouxel, O., Sohrin, Y., Stirling, C., Vance, D., Xue, Z., Zhao, Y., 2012. GEOTRACES IC1 (BATS) contamination-prone trace element isotopes Cd, Fe, Pb, Zn, Cu, and Mo intercalibration. Limnol. Oceanogr. Methods 10, 653–665.

Bruland, K.W., 1980. Oceanographic distributions of cadmium, zinc, nickel, and copper in the North Pacific. Earth Planet. Sci. Lett. 47, 176–198.

Carter, L., McCave, I.N., William, M.J.M., 2009. Circulation and water masses of the Southern Ocean: a review. In: Florindo, F., Siegert, M. (Eds.), Developments in Earth & Environmental Sciences. Elsevier, Amsterdam, pp. 85–114.

Cullen, J.T., Lane, T.W., Morel, F.M.M., Sherrell, R.M., 1999. Modulation of cadmium uptake in phytoplankton by seawater CO_2 concentration. Nature 402, 165–167.

Cullen, J.T., Chase, Z., Coale, K.H., Fitzwater, S.E., Sherrell, R.M., 2003. Effect of iron limitation on the cadmium to phosphorus ratio of natural phytoplankton assemblages from the Southern Ocean. Limnol. Oceanogr. 48, 1079–1087.

Cullen, J.T., Sherrell, R.M., 2005. Effects of dissolved carbon dioxide, zinc, and manganese on the cadmium to phosphorus ratio in natural phytoplankton assemblages. Limnol. Oceanogr. 50, 1193–1204.

Cullen, J.T., 2006. On the nonlinear relationship between dissolved cadmium and phosphate in the modern global ocean: Could chronic iron limitation of phytoplankton growth cause the kink? Limnol. Oceanogr. 51, 1369–1380.

de Baar, H.J.W., Buma, A.G.J., Nolting, R.F., Cadee, G.C., Jacques, G., Treguer, P.J., 1990. On Fe limitation of the Southern Ocean: Experimental observations in the Weddell and Scotia Seas. Mar. Ecol. Prog. Ser. 65, 105–122.

de Baar, H.J.W., de Jong, J.T.M., Bakker, D.CE., Löscher, B.M., Veth, C., Bathmann, U., Smetacek, V., 1995. Importance of iron for plankton blooms and carbon dioxide drawdown in the Southern Ocean. Nature 373, 412–415.

de Baar, H.J.W., Timmermans, K.R., Laan, P., de Porto, H.H., Ober, S., Blom, J.J., Bakker, M.C., Schilling, J., Sarthou, G., Smit, M.G., Klunder, M., 2008. Titan: A new facility for ultraclean sampling of trace elements and isotopes in the deep oceans in the international Geotraces program. Mar. Chem. 111, 4–21.

de Souza, G.F., Reynolds, B.C., Johnson, G.C., Bullister, J.L., Bourdon, B., 2012. Silicon stable isotope distribution traces Southern Ocean export of Si to the eastern South Pacific thermocline. Biogeosciences 9, 4199–4213.

Gault-Ringold, M., 2011. The marine biogeochemistry of cadmium: Studies of cadmium isotopic variations in the Southern Ocean. Doctoral dissertation. University of Otago, New Zealand.

Gault-Ringold, M., Adu, T., Stirling, C.H., Frew, R.D., Hunter, K.A., 2012. Anomalous biogeochemical behavior of cadmium in subantarctic surface waters: Mechanistic constraints from cadmium isotopes. Earth Planet. Sci. Lett. 341–344, 94–103.

Ho, T.-Y., Quigg, A., Finkel, Z.V., Milligan, A.J., Wyman, K., Falkowski, P.G., Morel, F.M.M., 2003. The elemental composition of some marine phytoplankton. J. Phycol. 39, 1145–1159.

Horner, T.J., Lee, R.B.Y., Henderson, G.M., Rickaby, R.E.M., 2013. Nonspecific uptake and homeostasis drive the oceanic cadmium cycle. Proc. Natl. Acad. Sci. USA 110, 2500–2505.

Klunder, M.B., Laan, P., Middag, R., de Baar, H.J.W., van Ooijen, J.C., 2011. Dissolved iron in the Southern Ocean (Atlantic sector). Deep-Sea Res., Part 2, Top. Stud. Oceanogr. 58, 2678–2694.

Lacan, F., Francois, R., Yongcheng, Y., Sherrell, R.M., 2006. Cadmium isotopic composition in the ocean. Geochim. Cosmochim. Acta 70, 5104–5118.

Lane, T.W., Saito, M.A., George, G.N., Pickering, I.J., Prince, R.C., Morel, F.M.M., 2005. A cadmium enzyme from a marine diatom. Nature 435, 42.

Lane, E.S., Semeniuk, D.M., Strzepek, R.F., Cullen, J.T., Maldonado, M.T., 2009. Effects of iron limitation on intracellular cadmium of cultured phytoplankton: Implications for surface dissolved cadmium to phosphate ratios. Mar. Chem. 115, 155–162.

Lee, J.G., Morel, F.M.M., 1995. Replacement of zinc by cadmium in marine phytoplankton. Mar. Ecol. Prog. Ser. 127, 305–309.

Löscher, B.M., de Jong, J.T.M., de Baar, H.J.W., 1998. The distribution and preferential biological uptake of cadmium at 6°W in the Southern Ocean. Mar. Chem. 62, 259–286.

Martin, J.H., Fitzwater, S.E., Gordon, R.M., 1990. Iron deficiency limits phytoplankton growth in Antarctic waters. Glob. Biogeochem. Cycles 4, 5–12.

Middag, R., de Baar, H.J.W., Laan, P., Cai, P.H., van Ooijen, J.C., 2011. Dissolved manganese in the Atlantic sector of the Southern Ocean. Deep-Sea Res., Part 2, Top. Stud. Oceanogr. 58, 2661–2677.

Middag, R., de Baar, H.J.W., Laan, P., Huhn, O., 2012. The effects of continental margins and water mass circulation on the distribution of dissolved aluminum and manganese in Drake Passage. J. Geophys. Res. C 01019, http://dx.doi.org/10.1029/2011JC007434.

Middag, R., de Baar, H.J.W., Klunder, M.B., Laan, P., 2013. Fluxes of dissolved aluminum and manganese to the Weddell Sea and indications for manganese colimitation. Limnol. Oceanogr. 58, 287–300.

Naveira Garabato, A.C., Jullion, L., Stevens, D.P., Heywood, K.J., King, B.A., 2009. Variability of Subantarctic Mode Water and Antarctic Intermediate Water in the Drake Passage during the late-twentieth and early-twenty-first centuries. J. Climate 22, 3661–3688.

Nelson, D.M., Smith Jr., W.O., 1991. Sverdrup revisited: critical depths, maximum chlorophyll levels, and the control of southern ocean productivity by the irradiance-mixing regime. Limnol. Oceanogr. 36, 1650–1661.

Nolting, R.F., de Baar, H.J.W., 1994. Behaviour of nickel, copper, zinc and cadmium in the upper 300 m of a transect in the Southern Ocean (57°–62°S, 49°W). Mar. Chem. 45, 225–242.

Orsi, A.H., Nowlin Jr., W.D., Whitworth III, T., 1993. On the circulation and stratification of the Weddell Gyre. Deep-Sea Res., Part 1, Oceanogr. Res. Pap. 40, 169–203.

Orsi, A.H., Whitworth III, T., Nowlin Jr., W.D., 1995. On the meridional extent and fronts of the Antarctic Circumpolar Current. Deep-Sea Res., Part 1, Oceanogr. Res. Pap. 42, 641–673.

Price, N.M., 2005. The elemental stoichiometry and composition of an iron-limited diatom. Limnol. Oceanogr. 50, 1159–1171.

Price, N.M., Morel, F.M.M., 1990. Cadmium and cobalt substitution for zinc in a marine diatom. Nature 344, 658–660.

Rafter, P.A., Sigman, D.N., Charles, C.D., Kaiser, J., Haug, G.H., 2012. Subsurface tropical Pacific nitrogen isotopic composition of nitrate: Biogeochemical signals and their transport. Glob. Biogeochem. Cycles 26, GB1003.

Ripperger, S., Rehkämper, M., 2007. Precise determination of cadmium isotope fractionation in seawater by double-spike MC-ICPMS. Geochim. Cosmochim. Acta 71, 631–642.

Ripperger, S., Rehkämper, M., Porcelli, D., Halliday, A.N., 2007. Cadmium isotope fractionation in seawater – A signature of biological activity. Earth Planet. Sci. Lett. 261, 670–684.

Rutgers van der Loeff, M.R., Cai, P.H., Stimac, I., Bracher, A., Middag, R., Klunder, M.B., van Heuven, S.M.A.C., 2011. [234]Th in surface waters: Distribution of particle export flux across the Antarctic Circumpolar Current and in the Weddell Sea during the GEOTRACES expedition ZERO and DRAKE. Deep-Sea Res., Part 2, Top. Stud. Oceanogr. 58, 2749–2766.

Santoso, A., England, M.H., 2004. Antarctic intermediate water circulation and variability in a coupled climate model. J. Phys. Oceanogr. 34, 2160–2179.

Sarmiento, J.L., Gruber, N., Brzezinski, M.A., Dunne, J.P., 2004. High-latitude controls of thermocline nutrients and low latitude biological productivity. Nature 427, 56–60.

Sievers, H.A., Nowlin Jr., W.D., 1984. The stratification and water masses at Drake Passage. J. Geophys. Res. 89, 10,489–410,514.

Sudre, J.S., Garçon, V., Provost, C., Sennéchael, N., Huhn, O., Lacombe, M., 2011. Short-term variations of deep water masses in Drake Passage revealed by a multiparametric analysis of the ANT-XXIII/3 bottle data. Deep-Sea Res., Part 2, Top. Stud. Oceanogr. 58, 2592–2612.

Sunda, W.G., Huntsman, S.A., 1997. Interrelated influence of iron, light and cell size on marine phytoplankton growth. Nature 390, 389–392.

Sunda, W.G., Huntsman, S.A., 1998. Interactions among Cu^{2+}, Zn^{2+}, and Mn^{2+} in controlling cellular Mn, Zn, and growth rate in the coastal alga Chlamydomonas. Limnol. Oceanogr. 43, 1055–1064.

Sunda, W.G., Huntsman, S.A., 2000. Effect of Zn, Mn, and Fe on Cd accumulation in phytoplankton: implications for oceanic Cd cycling. Limnol. Oceanogr. 45, 1501–1516.

Whitworth III, T., Nowlin Jr., W.D., 1987. Water masses and currents of the Southern Ocean at the Greenwich Meridian. J. Geophys. Res. 92, 6462–6476.

Xu, Y., Feng, L., Jeffrey, P.D., Shi, Y., Morel, F.M.M., 2008. Structure and metal exchange in the cadmium carbonic anhydrase of marine diatoms. Nature 452, 56–62.

Xue, Z., Rehkämper, M., Schönbächler, M., Statham, P.J., Coles, B.J., 2012. A new methodology for precise cadmium isotope analyses of seawater. Anal. Bioanal. Chem. 402, 883–893.